Electrical Breakdown Spots in Metal-Aluminum Oxide-Metal Structures

Herbert Kliem and Kapil Faliya
Saarland University
Campus A5 1
66123 Saarbruecken, Germany

ABSTRACT

Metal-aluminum oxide-metal structures are prepared by evaporation in vacuum on silicon wafers using Au, Cu or Pd on top and Al as bottom electrode. The aluminum oxide layer is deposited by electron beam evaporation with a thickness of 200 nm. The diameter of the top electrode is varied between 0.1 and 1.9 mm. Capacitance measurements reveal a relaxational dielectric permittivity as expected for aluminum oxide. Applying ramp voltages results in single breakdown spots on the electrode before the structure finally becomes conductive. The breakdown spots, as characterized with an AFM, are in the form a crater, reaching 500 nm into the silicon. However, for the smallest electrode, the calculated electrostatic energy stored in the capacitance is not high enough to form the craters.

Index Terms — **metal-aluminum oxide-metal structures, partial electrical breakdown, breakdown spots, AFM, hydrogen, cold fusion**

1 INTRODUCTION

ELECTRICAL breakdown of dielectrics has been reported in countless articles and in many books. Even the literature of breakdown in aluminum oxide can hardly be overviewed. An important book which lays down basics is certainly the one by O'Dwyer [1]. Here it is already pointed out that the breakdown field in aluminum oxide increases with decreasing thickness of the sample. Evaluating his data, the tendency to reach a plateau below a thickness of 100 nm can be seen. This plateau is clearly shown by Neusel and Schneider [2]. They report for aluminum oxide with a thickness below 100 nm a constant breakdown field of about 1 MV/cm. A similar breakdown field of 1.2 MV/cm is found for aluminum oxide with a thickness of 200–800 nm produced by a wet chemistry route [3]. In amorphous aluminum oxide films of thickness 210 nm the breakdown field is about 4 MV cm^{-1} in a dry sample and 7.6 MV/cm in a hydrated sample [4]. An ultrathin Al_2O_3 film of only 0.7 nm thickness was investigated in [5]. The authors find a breakdown field of 11 MV/cm.

Thus the above mentioned plateau of the breakdown field below 100 nm becomes questionable. The classical route to produce aluminum oxide is the anodic oxidation as used in electrolyte capacitors. Here De Wit and Crevecoer find breakdown fields of 9 MV/cm for film thicknesses between 23 and 169 nm [6]. Another route is the preparation of Al_2O_3 by thermally oxidizing AlN. For all thicknesses of 25 to 435 nm the breakdown strength is about 5 MV/cm [7]. Al_2O_3 can also be obtained by atomic layer deposition [8]. The breakdown field here is 7 MV/cm. Voigt and Sokalowski prepared Al_2O_3 films of thickness 160 nm on ITO covered glass by magnetron sputtering. Before final breakdown appears at about 1 MV/cm spikes in the current indicate partial breakdowns [9]. Our measurements reveal breakdown fields of 1.8 to 4.25 MV cm^{-1} in films with thickness 200 nm. This is in line with the values reported in the literature. Another test method is the application of a step voltage and the measurement of the time to breakdown [10] or the charge to breakdown in SiO_2 [11]. To describe the statistical nature of breakdown events also distribution functions like the Weibull-distribution are used [12].

We employ the following approach: To a flat metal-insulator-metal (MIM) structure on silicon a ramp voltage is applied. Before a final breakdown of the sample occurs single breakdown spots are visible at the surface of the top electrode. Inspection of the spots with an optical microscope as well as with an atomic force microscope (AFM) reveals crater like holes. On top the diameter of the holes is about 10 μm or less. Their depth reaches into the silicon base.

The appearance of breakdown spots in metalized thin polymer films is known since long times [13] and has been analyzed theoretically for example by Tortai *et al* [14]. After the breakdown the capacitor recovers. This so called self-healing effect takes place in the dielectric for instance at impurities and the heat production evaporates the electrodes at both sides. Instead, here the electrode is burnt away on the top and at the bottom side a crater is built into the thick electrode material which is in the main focus of this paper.

Manuscript received on 23 September 2019, in final form 9 March 2020, accepted 10 March 2020. Corresponding author: H. Kliem.

DOI: 10.1109/TDEI.2020.008526

2 SAMPLE PREPARATION AND MEASUREMENT TECHNIQUE

Samples were prepared on a flat silicon wafer. The wafer is covered with thermally evaporated copper of 600 nm thickness and aluminum of 40 to 80 nm thickness. Then, without breaking the vacuum ceramic aluminum oxide from Chempur with a purity of 99.99% is evaporated to form an aluminum oxide film on the aluminum surface. This step is carried out by electron beam evaporation in an oxygen atmosphere of 10^{-6} mbar. The evaporation rate was 0.1 nm per second measured by a quartz crystal balance. After achieving a standard film thickness of 200 nm a shadow mask was shifted under the sample. Also this step was performed in vacuum. The shadow mask with holes of diameter 0.1 to 1.9 mm allows the evaporation of the top electrodes. Gold, copper and palladium top electrodes with a thickness of about 80 nm were prepared on the aluminum oxide surface.

The contact to the sample was accomplished with a homemade station using an elastic needle with a spring. All measurements were carried out at ambient atmosphere. To assess the quality of the samples first the capacitance-frequency C(f) curves were probed with a LCR-meter. Using a source meter, a ramp voltage with a speed 1V/s was applied to the sample. So the experiments are performed in direct-current condition. The source meter has an internal resistor of 300 kΩ to protect the instrument against short circuits. This implies that the resistor is always in series to the sample and limits the current flow. The current to the sample is measured during the application of the voltage ramp and recorded simultaneously. In parallel to the voltage application and current measurement the surface of the electrode was inspected by an optical microscope. Images were recorded with a speed of 20 frames per second using a CCD camera. The breakdown spots were characterized with respect to lateral size and depth using an AFM.

3 EXPERIMENTS

All experiments are conducted at room temperature in environmental conditions. First measurements are carried out using the structure with the Cu-electrode of diameter 1.9 mm. Au electrodes yield almost the same result. The ramp voltage is applied and the current to the structure is measured (Figure 1). After a slow increase of the current we find a final breakdown at 85 V corresponding to 4.25 MV cm^{-1} indicated by the straight line. This line refers to the 300 kΩ internal resistor of the source. Although in the current record only 21 peaks are visible we find more than 140 breakdown spots on the electrode after the voltage ramp experiment. This is illustrated with the optical image of the electrode depicted with Figure 2. The breakdown events start to appear at fields above 1 MV cm^{-1}.

Within the small areas where the electrode apparently is burned away tiny dark dots can be seen. A closer look to the breakdown spots is possible with the tip of an atomic force microscope. Figure 3a shows one of the holes from the electrode depicted in Figure 2.

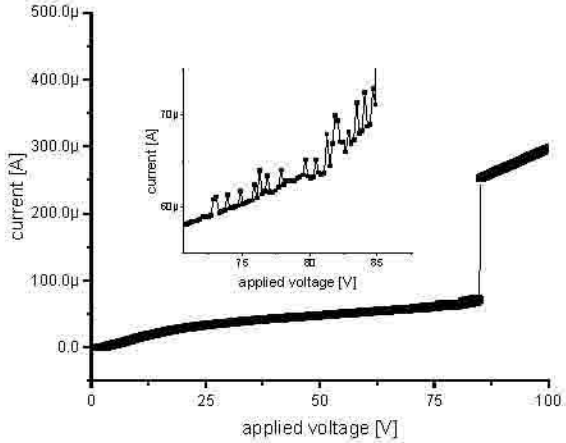

Figure 1. The current-voltage curve of a structure with an electrode of 1.9 mm in diameter recorded using a ramp with 1V/s. Peaks in the current only appear for voltages above 70 V. The total number of recorded peaks is 21.

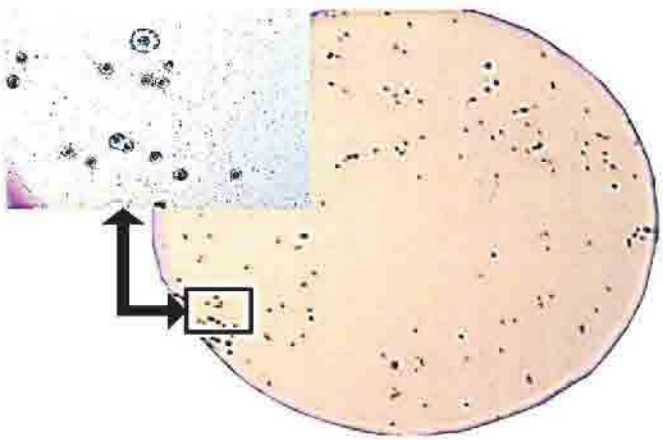

Figure 2. The optical image of the electrode used for Figure 1 with 1.9 mm diameter after voltage application. More than 140 breakdown spots are found.

The different colours give an idea of the form of this crater like hole. The light parts indicate heightenings and the dark parts indicate deepenings. A more quantitative evaluation is possible using the cross section through the crater shown in Figure 3b.

The diameter of the hole is approximately 7 µm, the depth is about 1 µm. Considering the thicknesses of the top electrode with 85 nm, the oxide with 200 nm, the Al bottom layer with 80 nm and the copper bottom layer with 600 nm it becomes evident that the hole reaches down to the silicon substrate. The other spots have a similar appearance.

Next, electrodes with a diameter of 1.1 mm were investigated. Again we find several breakdown spots. They appear at voltages below 75 V where the structure finally breaks down. By AFM measurement a single breakdown spot and its cross section is depicted in Figures 4a and 4b.

The hole has at the surface a diameter of about 3 µm while the electrode is burnt away on a diameter of about 9 µm. The depth of the crater with a maximum of 1.2 µm reaches again into the silicon substrate. The silicon is melt and evaporated down to a depth of about 300 nm. The simultaneously recorded

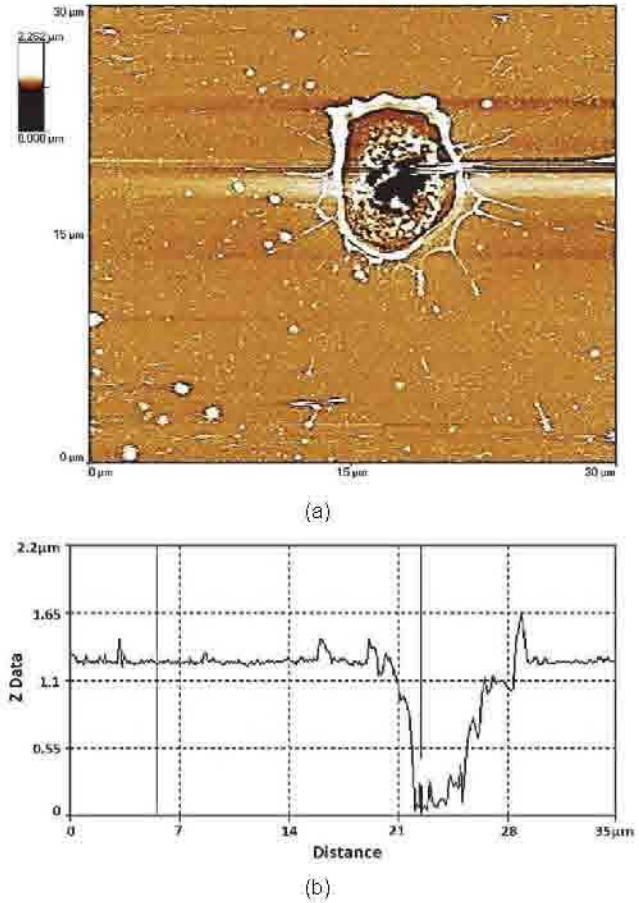

Figure 3. (a) An AFM image of one of the holes on the electrode depicted in Figure 2. Electrode diameter is 1.9 mm. Light regions denote heightenings, dark regions denote deepenings. The scale is given on the upper left side. (b) The cross selection of the hole from Figure 3a. The measured curve is the surface of the sample with the breakdown spot.

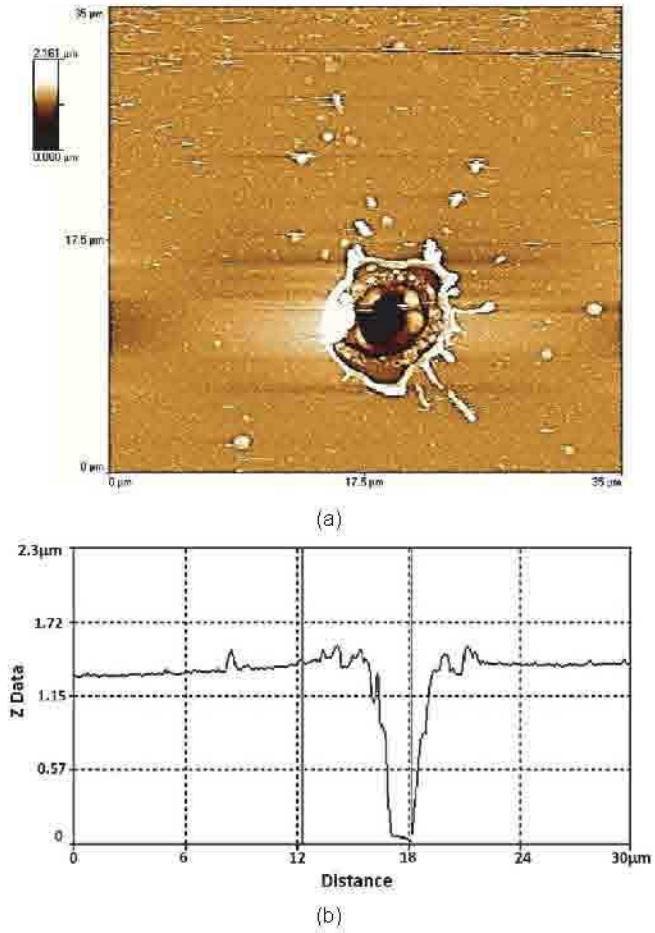

Figure 4. (a) An AFM image of a breakdown crater on an electrode with 1.1 mm diameter. Colors represent different heights. Scale: see upper left side. (b) The cross section of the crater from Figure 4a

I(U) curve and the optical microscope movie demonstrate that this hole is created at about 60 V applied. The movie also shows that the holes are formed at different voltages one by one.

Finally a structure with an electrode diameter of 0.1 mm is investigated. The capacitance – frequency curve (Figure 5) exhibits a steady decrease of the capacitance with increasing frequency for 20 Hz ≤ f ≤ 1 MHz.

This is due to a relaxational process with a distribution of relaxation times as discussed and interpreted in former publications [15, 16]. At a frequency of 3 kHz we find a permittivity ε_r = 7.9. At this frequency a voltage sweep is carried out from U = 0 to + 40V, + 40 to – 40V, and - 40 towards + 40V where the structure has a final breakdown at + 36 V. Figures 6a and 6b depicts the C(V) curve as well as the tanδ(V) curve. The optical inspection of the electrode yields only one single breakdown spot. With the appearance of this spot the area of the electrode decreases by about 5%. Since a step down of the capacitance during the sweeps before breakdown is not observed the spot must appear at the breakdown voltage of 36 V. Figure 7 shows the AFM records of the crater (Figure 7a) and the depth profile (Figure 7b). Again the electrode around the hole is burnt away now on a diameter of about 20 µm (Figure 7a).

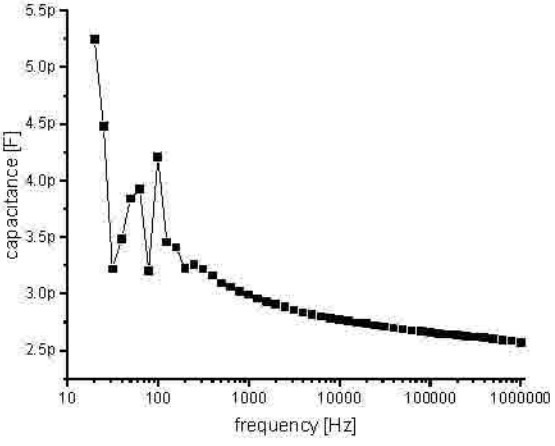

Figure 5. The C(f) measurement at a MIM-structure with 0.1 mm diameter.

Figure 7b depicts the cross section of the breakdown spot as well as the layers Cu, AlOx, Al, Cu and the silicon surface. It is visible that the breakdown spot extends 500 to 600 nm deep into the silicon wafer.

Both the final breakdown voltage and the appearance of the spots seem not to be significantly dependent on the electrode area. The ratio of largest to smallest area is $(1.9)^2/(0.1)^2 = 361$.

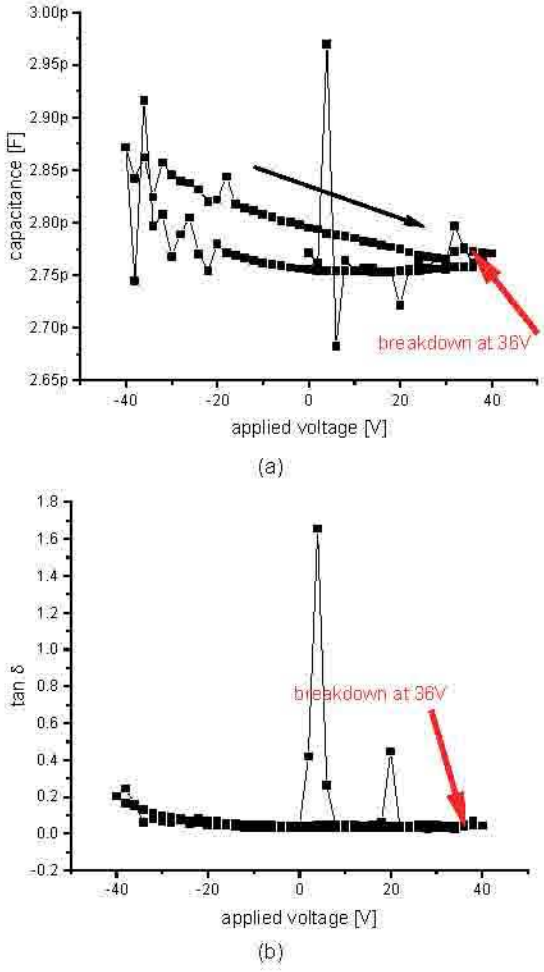

Figure 6. (a) C(V) curve for the MIM structure with 0.1 mm diameter. Breakdown appears at 36 V. (b) Tan δ (V) curve for the MIM structure 0.1 mm in diameter.

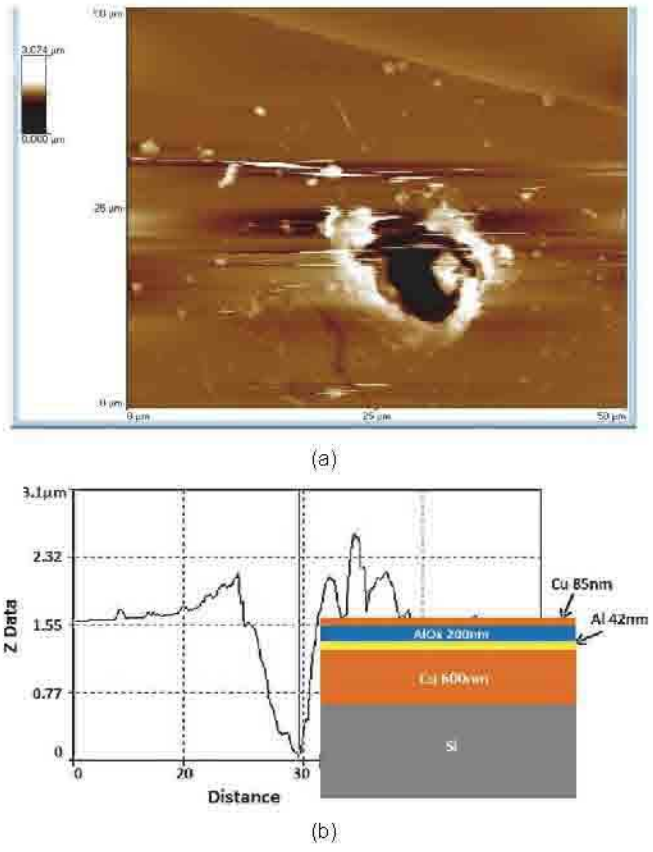

Figure 7. (a) Breakdown crater at the electrode with 0.1 mm diameter. The electrode around the hole is burnt away for about 20 µm in diameter. (b) The corresponding cross section of the crater from Figure 7a. The structure of the sample with the different layers is depicted.

An almost homogeneous field is expected in the dielectric film even for the smallest electrode since the ratio of diameter and film thickness here is 10^{-4}m/$2{\cdot}10^{-7}$m = 500.

Final breakdown voltages are between 36 and 85V. However, to perform a meaningful statistical analysis of the breakdown voltages there are not enough measurement data. In this paper we focus on the depth of the breakdown spots.

A last experiment was carried out using a Pd-electrode (Figure 8). After voltage application we find an approximately three to four times higher density of holes than in the case of a Cu-electrode. A similar observation was reported by Ball [17]: Pd-electrodes can exhibit an electrochemical mechanical damage upon H_2 evolution. Before electrochemistry the Pd cathode is uniform and after electrochemistry the Pd cathode is speckled because of high H flux and H_2 evolution. When the solid electrolyte BZCY (ceria- and yttria-doped barium zirconate) is coated with a Pd film as electrode, the Pd film delaminates, and the ceramic grains are fractured and ejected.

The breakdown spot depicted in Fig. 7 was achieved with the connection of the sample to a LCR-meter in biasmode with a low internal resistance while the spots in Figures 3 and 4 were measured with a source having an internal resistor of 300

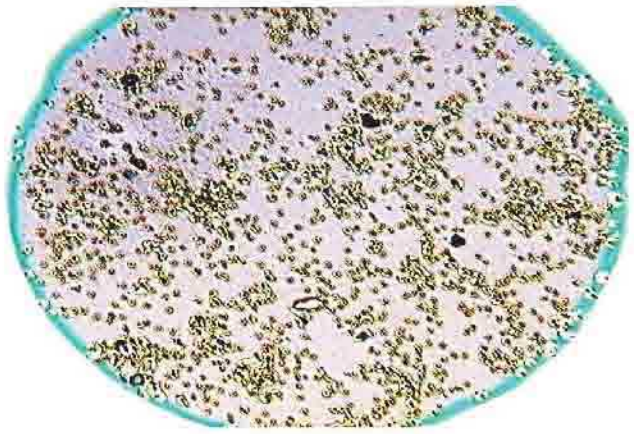

Figure 8. Optical image of a Pd-electrode with diameter 1.1 mm after voltage application.

kΩ as mentioned above. In spite of the different resistivities the breakdown craters have a similar appearance. Further, it is seen with Figure 8 that breakdown craters also at the blue-green edge of the Pd-electrode are found. This colour indicates a very thin Pd-film resulting from the edge of the shadow mask. Thin Pd films can exhibit resistivities of 10^2 Ωm while the bulk value is 10^{-7}Ωm which increases gradually with decreasing thickness [18]. Although we have not measured these spots at the edge by the AFM, from their optical

appearance they seem to be similar to the spots in the electrode's center. Thus, the electrode resistivity seems not to be of primary importance for the spots.

4 DISCUSSION

Several observations have to be interpreted:

I) The local breakdown spots can be initiated by defects in the oxide. During the formation of the spots current spikes in the external circuit are not detected for each hole. This can be interpreted by the following mechanism: The breakdown channel appears and produces heat. This heat burns away the electrode around the channel. Only the partial capacitance in the electrode's area that is burnt away has discharged. Now this area is no longer connected to the circuit and cannot be reloaded. This is illustrated with the equivalent circuit in Figure 9. Before breakdown there exists the electrode represented by a number of small resistors and the dielectric represented by small capacitances. At the breakdown moment a short circuit is found which immediately burns away the electrode's area around the breakdown channel. A hole is formed and no capacitance can be reloaded. Similar observations of breakdown spots in aluminum oxide were reported in [19]. The authors find holes in the electrode like in our Figure 2 detected optically and by scanning electron microscopy. They also observe sharp tips in the holes which in our case result in the craters depicted in Figures 3b, 4b, 7b. They explain the absence of current spikes in their measurements with the short period of the breakdown event of the estimated 10^{-6} to 10^{-5} s which could not be resolved.

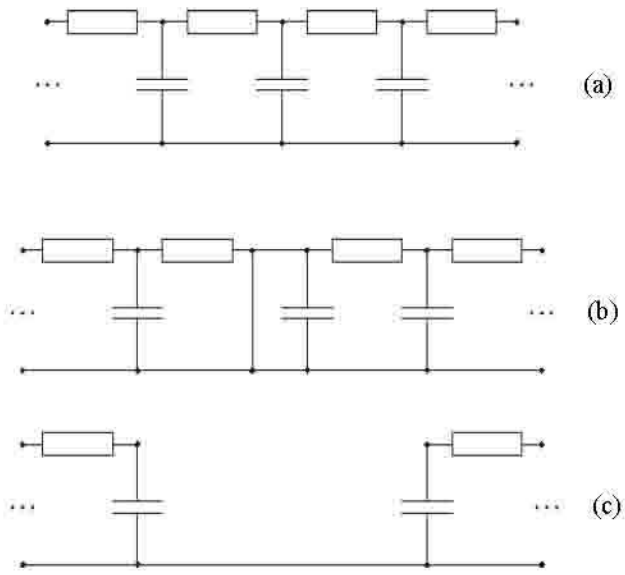

Figure 9. An equivalent circuit representation of the formation of a hole. The electrode is represented by resistors, the dielectric is represented by capacitors; (a) before breakdown, (b) short circuit in the moment of breakdown, and (c) burnt hole.

II) The size of the breakdown craters is up to a certain point independent of the electrode's area. The ratio of largest to smallest electrode area is $(1.9)^2 / (0.1)^2 = 361$. Therefore the energy dissipated in the breakdown event cannot be related to the electrostatic energy W_{est} stored in the capacitance C which is proportional to the electrode's area,

$$W_{est} = \frac{1}{2} C U^2 \tag{1}$$

This observation is in line with point I). If only the area close to the breakdown channel discharges the breakdown crater is independent of the electrode's area.

III) An estimate for the energy necessary to produce the breakdown crater shall be derived. This energy is compared to the electrostatic energy.

It is assumed that the crater is formed by melting and evaporating the craters material. This consists from top to bottom of Cu, AlOx, Al, Cu and Si as illustrated in Figure 7b. The volume of each material is approximated by a frustum of a cone for each layer with diameters taken from Figure 7b. Using the melting temperatures, the specific heat capacitances and masses as well as the heat of fusion for each material we find an energy of around $W_m \approx 10 \cdot 10^{-8}$J necessary to melt the crater's volume. If the material is evaporated the corresponding heats of vaporization and the evaporation temperatures must be taken into account. Then a total energy for the evaporation of the hole $W_{eva} \approx 70 \cdot 10^{-8}$J is required.

These two thermal energies are compared now to the electrostatic energy stored in the MIM structure with 0.1 mm electrode diameter.

From Figure 5 a high frequency capacitance of $C \leq 3$pF can be read out. The electrostatic energy at the breakdown voltage of 36V is therefore using Equation (1) $W_{est}^{(1)} \approx 0.2 \cdot 10^{-8}$J. Only this electrical energy is available. But this energy is 50 times less than the melting energy and 350 times less than the evaporation energy:

$$\frac{W_m}{W_{est}^{(1)}} \approx 50 \quad and \quad \frac{W_{eva}}{W_{est}^{(1)}} \approx 350 \tag{2}$$

If the considerations in points I) and II) are correct then only the electrostatic energy in the vicinity of the breakdown center can be involved. This energy $W_{est}^{(2)}$ stored in an area of about 20 µm diameter is by a factor of 0.04 smaller than the electrostatic energy stored in the whole electrode of 100 µm diameter. Then the ratios of available electrostatic energy and thermal energies are even higher. We find then

$$\frac{W_m}{W_{est}^{(2)}} = 1250 \quad and \quad \frac{W_{eva}}{W_{est}^{(2)}} = 8750 \tag{3}$$

It is therefore concluded that the electrical breakdown triggers an event which releases much more energy than stored in the electrical field. This is in analogy to a spark which triggers an explosion. In our former publication [16] we could prove that hydrogen is present in the aluminumoxide. Also, Pd can absorb hydrogen from the atmosphere. The hydrogen then diffuses into the oxide. Since using the Pd-electrode much more breakdown spots are observed (Figure 8), it is possible

that hydrogen is involved in the partial breakdown processes. Depth and volume of these holes are comparable to the holes found using Cu-electrodes. Probably the hot breakdown channel triggers local hydrogen explosions on the microscale which deliver the energy necessary to produce the craters.

5 CONCLUSIONS

Single breakdown spots are observed in metal-aluminum oxide-metal structures. By the breakdown event channels and craters are formed in the structure. The energy required to form these holes is much higher than the electrostatic energy stored in the MIM structure. It is therefore concluded that the breakdown event with its high channel temperatures triggers a second process which delivers the required energy. Since the number of breakdown spots at structures with a Pd electrode is by a factor of three to four higher than at structures with Cu electrodes it is conjectured that hydrogen explosions on the microscale are involved in the breakdown process delivering the energy for the creation of the craters.

It remains an open question if these processes are somehow related to the supposed cold fusion reported 30 years ago [20] and recently discussed in [17].

REFERENCES

[1] J. J. O'Dwyer, *The Theory of Electrical Conduction and Breakdown in Solid Dielectrics*, Clarendon Press Oxford, 1973.

[2] C. Neusel and G. A. Schneider, "Size dependence of the dielectric breakdown strength from nano to millimeter scale," J. Mechanics and Physics of Solids vol. 63, pp. 201–213, 2014.

[3] M. Yao and W. Shan, "Dielectric behavior of alumina thin film under high DC electric field prepared by sol-gel method," J. of Advanced Dielectrics, vol. 03, no. 03, pp. 1350017, 2013.

[4] M. Jao *et al*, "Anodic Oxidation in aluminum electrode by using hydrated amorphous aluminum oxide film as solid electrolyte under high electric field," Appl. Mater. Interfaces, pp. 11100-7, 2016.

[5] N.P. Magtoto *et al*, "Dielectric breakdown of ultrathin aluminum oxide films induced by scanning tunneling microscopy," Appl. Phy. Lett. vol. 77, pp. 2228–2230, 2000.

[6] H. J. Dewitt and C. Crevecoer, "The dielectric breakdown of anodic aluminum oxide," Phys. Lett. vol. 50 A, pp. 365–366, 1974.

[7] J. Kolodzey *et al*, "Electrical conduction and dielectric breakdown in aluminumoxide insulators on silicon," IEEE Trans. Dielectr. Electr. Insul., 47, pp. 121–128, 2000.

[8] J. Yota, H. Shen, and R. Ramanathan, "Characterization of atomic layer deposition HfO_2, Al_2O_3, and plasma-enhanced chemical vapor deposition Si_3N_4 as metal-insulator-metal capacitor dielectric for GaAs HBT technology," J. Vac. Sci. Technol., A 31 (1), pp. 01A134-1-01A136-9, 2013.

[9] M. Voigt and M. Sokolowski, "Electrical properties of thin rf sputtered aluminum oxide films," Mat. Sci. and Engineering, B vol. 109, (1), pp. 99–103, 2004.

[10] N. Klein and M. Albert, "Electrical breakdown of aluminumoxide films flanked by metallic electrodes," J. Appl. Phys. vol. 53, pp. 5840–5850, 1982.

[11] J. F. Verweij and D. R. Wolters, *Insulating Films on Semiconductors*, North-Holland, Elsevier Science Publishers B.V., 1983.

[12] E. Tuncer *et al*, "On dielectric breakdown statistics," J. Phys. D, 39, pp. 4257–4268, 2006.

[13] H. Heywang, "Physical and chemical processes in self-curing plastic capacitors," Colloid Polym. Sci. 254, pp. 138–47, 1976.

[14] J. H. Tortai, A. Denat, and N. Bonifaci, "Self-healing of capacitors with metallized film technology: experimental observations and theoretical model," J. of Electrostatics, 53, pp. 15–169, 2001.

[15] L. Kankate, A. Gratsov, and H. Kliem "Nonlinear relaxational polarization in aluminum oxide," IEEE Trans. Dielectr. Electr. Insul., vol. 22, no 2, pp. 1220–1231, Apr. 2015.

[16] L. Kankate, C. Nies, W. Possart, and H. Kliem, "Role of hydrogen, oxygen and composite formation in relaxational polarization of hafnium oxide and aluminum oxide," IEEE Trans. Dielectr. Electr. Insul., vol. 25, no. 4, pp. 1508–1517, Aug. 2018.

[17] P. Ball, "Material advances result from study of cold fusion," MRS BULLETIN, 44, pp. 833–836, 2019.

[18] M. Kühn, M. Aeron, R. Florange and H. Kliem, "On the temperature stability of integrated MIS low-pass filter structures," Sol. St. Electronics, 51, pp. 931–935, 2007.

[19] A. Belkin, A. Bezryadin, L. Hendren, and A. Hubler, "Recovery of alumina nanocapacitors after high voltage breakdown," Scientific Reports, 7:932, pp. 1–7, 2017.

[20] M. Fleischmann, and S. Pons, "Electrochemically induced nuclear fusion of deuterium," J. Electroanal. Chem. Interfacial Electrochem., 261, pp. 301–308, 1989.

Herbert Kliem received the diploma in electrical engineering with the subject area solid state electronics and the degree Dr.-Ing., both at the University of Technology Aachen, Germany. In 1991, he joined the Technical University Hamburg-Harburg and achieved the qualification as a university lecturer. Since 1996, he has been full-time professor and head of the Institute of Electrical Engineering Physics at the Saarland University.

Kapil Faliya was born in Jamnagar, Gujarat, India in 1988. He received the B. Eng. degree in aeronautical engineering from the Gujarat University, India in 2009 and the M.Sc. degree in material science and engineering from the Kiel University, Germany in 2014. From 2011 until 2013, he worked at the Germany Aerospace Center, Braunschweig, Germany as a student research assistant. Since 2013, he has been working as a PhD at the Institute of Electrical Engineering Physics, Saarland University, Germany.